JOURNAL OF SPACECRAFT AND ROCKETS
Vol. 56, No. 6, November–December 2019

Rapid Modeling of Electrostatic Forces and Torques Considering Dielectrics

Joseph Hughes* and Hanspeter Schaub†
University of Colorado at Boulder, Boulder, Colorado 80309

DOI: 10.2514/1.A34413

Spacecraft can charge naturally to tens of kilovolts in geosynchronous orbit due to their interactions with the space plasma and the sun. This charging can cause forces and torques that can perturb the orbits of uncontrolled debris objects or be used as a form of touchless actuation in an active charging multicraft formation. Prior work for electrostatic force and torque prediction has developed rapid and accurate methods for conducting spacecraft using the multisphere method (MSM). This paper extends the MSM for spacecraft composed of conductors and dielectrics. It is found that, for some spacecraft and charging regimes, dielectrics can be neglected without introducing significant errors. For the cases that require dielectrics be considered, the MSM is augmented to include dielectric point charges as well as conducting spheres that are placed and sized by a numerical optimizer. Designs are developed that perform better than an average of 2% error for all spacecraft and charging scenarios considered.

Nomenclature

C_{MD}	=	mutual dielectric capacitance
C_S	=	self-capacitance, F
$\boldsymbol{E}$	=	electric field, N/C
N	=	number of operations
q	=	charge, C
R	=	sphere radius, m
$r_{i,j}$	=	intersphere distance, m
$[S]$	=	elastance matrix, F^{-1}
V	=	voltage, V
ϵ_0	=	vacuum permittivity; $\approx 8.85418782 * 10^{-12}$, F/m
χ_{MD}	=	mutual dielectric elastance, m
χ_S	=	self-elastance, F/m

I. Introduction

IN THE geosynchronous Earth orbit (GEO) regime, satellites charge to very high voltages: sometimes as dramatic as −19 kV [1]. This charging causes small forces and torques on the body due to interactions with Earth's magnetic field, which changes the orbits of some uncontrolled lightweight debris objects through the Lorentz force [2–5]. If nearby spacecraft use active charging such as electron and ion guns, larger forces and torques are felt between the craft. This enables novel Coulomb formation-flying missions [6–8]. These forces can also be used for touchless reorbiting of GEO debris to its graveyard orbit in a matter of months using the electrostatic tractor [9,10]. If a spacecraft has a nonsymmetric charge distribution, it also experiences torques, which can be harnessed for touchless despin before servicing or grappling [11–13].

There are many separate challenges to electrostatic actuation, such as prescribing the appropriate electron and/or ion beam current and voltage; sensing the voltage, position, and attitude of a passive space object; and designing control laws that perform well for either tugging or despinning. To design and implement stable and performant control laws in any of the aforementioned mission scenarios, accurate and fast methods are needed to predict the force and torque on both spacecraft using only in situ measurements such as the voltage of each craft and their relative separation and attitude. Accuracy is important because under- or overprediction can seriously harm performance, or lead to a collision [14]. Speed is important because the force and torque must be predicted in real time by the flight computer. This paper discusses how to predict electrostatic force and torque for a body that is composed of conductors and dielectrics, as shown in Fig. 1.

There are many methods for force and torque prediction, ranging from very accurate but much slower than real-time methods such as the finite element analysis (FEA) or faster and more scalable methods such as the method of moments (MOM) [15] or boundary element method. Prior work explores using the Galerkin method to model forces between two dielectric spheres [16]. A relatively new scheme for electrostatic force and torque prediction is the multisphere method (MSM) [17]. The MSM is very similar to the MOM in that an elastance matrix is populated and then inverted to find the charge distribution. The Coulomb force is applied from every discretized charge on one body to every discretized charge on the other body. The MSM differs from the MOM in that the elements of the elastance matrix are tuned to match force and torque created by a higher-fidelity method rather than from first principles. Because of this tuning, the MSM can predict forces and torques with only a few percent error using only three to four spheres for a two-craft system [18,19], but it requires a truth model from which to optimize. It is a robust method for force and torque prediction for conducting systems; however, not all spacecraft are continuously conducting. Recent work [20] investigated how to modify the MSM to account for dielectrics and found very small impacts when the dielectric lies directly on top of the conducting surface of the spacecraft.

Most spacecraft are built to be continuously conducting to avoid differential charging and arcing. However, some of the conducting covering may degrade with time and lose its conductivity. Two scenarios for which this may occur involve the coverglass coating on the solar panels and the multilayer insulation (MLI). Solar panels require a glass cover to protect from proton radiation, and there is usually a conductive clear coating over the glass; however, this coating may degrade or flake off, and can leave sections of the nonconductive glass exposed. MLI also usually has a gold or aluminum coating, but this may flake off or otherwise degrade. Additionally, some spacecraft are not built as fully conducting to begin with, and they will have large dielectric portions. In the case of coverglass and MLI, there is a thin layer (10–100 μm) of dielectric sitting directly on top of a conductor connected to the spacecraft ground. However, in an effort to save weight, some spacecraft have the MLI wrapped around a skeleton frame with very little area of the MLI touching the conducting bus.

Received 16 October 2018; revision received 30 March 2019; accepted for publication 15 April 2019; published online 19 June 2019.

*Department of Aerospace Engineering, 429 UCB; Joseph.Hughes@Colorado.edu.

†Department of Aerospace Engineering, 429 UCB; Hanspeter.Schaub@Colorado.edu

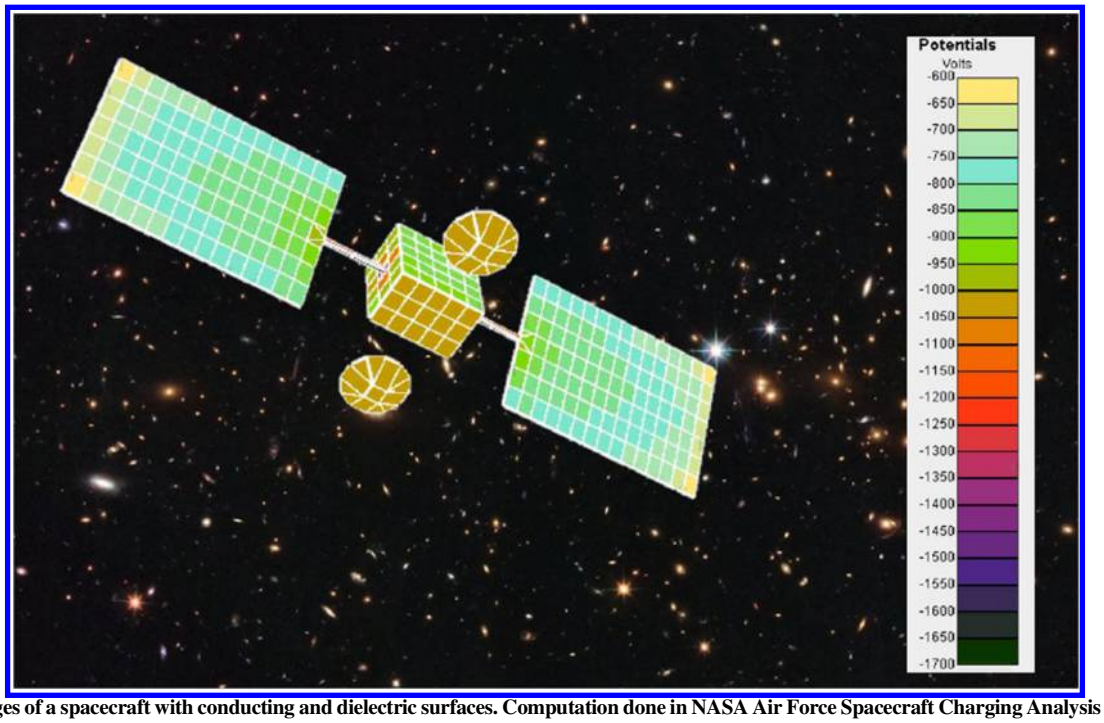

Fig. 1 Voltages of a spacecraft with conducting and dielectric surfaces. Computation done in NASA Air Force Spacecraft Charging Analysis Program-2k.

II. Problem Statement

The multisphere method was originally created as a fast way to predict the electrostatic force and torque between conductors [17]. It is very similar to the method of moments, but rather than the elements of the elastance matrix being derived from first principles, they are hand tuned to match force, torque, or Electric (E) fields predicted by a higher-fidelity model like the FEA or MOM.

As shown in Fig. 2, the MSM approximates a spacecraft as a collection of spheres with variable positions and radii. The voltage on any sphere is a function of both its own charge and the charge of all nearby spheres. If these spheres are far enough away to be approximated as point charges, the voltage is given by [17]

$$V_i = \frac{1}{4\pi\epsilon_0}\frac{q_i}{R_i} + \sum_{j=1, j\neq i}^{n} \frac{1}{4\pi\epsilon_0}\frac{q_j}{r_{i,j}} \tag{1}$$

where q_i and R_i are the charge and radius of the ith sphere, respectively, $\rho_{i,j}$ is the center-to-center distance between spheres i and j, and ϵ_0 is the permittivity of free space constant. If the voltages of each sphere are given by $\boldsymbol{V} = [V_1, V_2, \ldots, V_n]^T$ and the charges are given by $\boldsymbol{q} = [q_1, q_2, \ldots, q_n]^T$, the relationship between the two is

$$\boldsymbol{V} = [S]\boldsymbol{q} \tag{2}$$

where $[S]$ is the elastance matrix defined as follows:

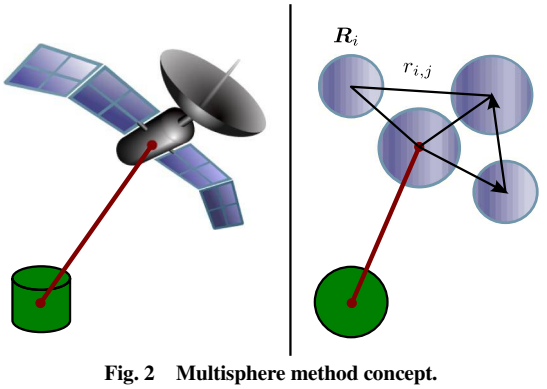

Fig. 2 Multisphere method concept.

$$[S] = \frac{1}{4\pi\epsilon_0}\begin{bmatrix} 1/R_1 & 1/r_{1,2} & \cdots & 1/r_{1,n} \\ 1/r_{2,1} & 1/R_2 & \cdots & 1/r_{2,n} \\ \vdots & \vdots & \ddots & \vdots \\ 1/r_{n,1} & 1/r_{n,2} & \cdots & 1/R_n \end{bmatrix} \tag{3}$$

If the voltage is known, the linear system can be solved for the charges $\boldsymbol{Q}$. Combining the charges with the locations of the spheres allows the force and torque to be computed. In a flat E field, the net force and torque are

$$\boldsymbol{F} = \boldsymbol{E}\sum_{i=1}^{n} Q_i \qquad \boldsymbol{L} = \sum_{i=1}^{n} Q_i\boldsymbol{\rho}_i \times \boldsymbol{E} \tag{4}$$

for an MSM model with n spheres, where $\boldsymbol{\rho}_i$ points from the origin to sphere i. In a detumbling scenario, another spacecraft (with m spheres) is nearby and the Coulomb force is applied between each pair of spheres:

$$\boldsymbol{F} = \sum_{i=1}^{n}\sum_{j=1}^{m} \frac{Q_i Q_j \boldsymbol{r}_{ij}}{4\pi\epsilon_0 r_{ij}^3} \tag{5}$$

The torque is then

$$\boldsymbol{L} = \sum_{i=1}^{n}\sum_{j=1}^{m} \boldsymbol{\rho}_i \times \frac{Q_i Q_j \boldsymbol{r}_{ij}}{4\pi\epsilon_0 r_{ij}^3} \tag{6}$$

This process has been used successfully for modeling spacecraft with complex geometries as close as a few craft diameters with errors of a few percent [19].

This paper will investigate two separate questions. First, under what circumstances do dielectrics have to be accounted for to accurately model the force and torque? Second, how can the MSM be modified to account for dielectrics? To answer the first question, four different template spacecraft are considered under three different charging scenarios. Once situations that require modeling the dielectric effects are identified, a modification to the conducting MSM is presented and tested on the template spacecraft.

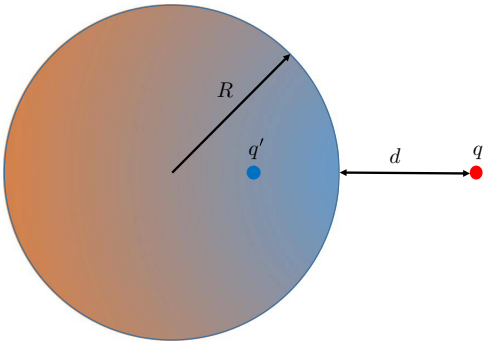

Fig. 3 Method of images concept illustration.

III. Method of Images Analysis

To gain some analytical insight into the first question of when dielectrics need to be accounted for, first consider a much simpler system using the method of images (MOI) [21–23]. If a positive point charge is held a distance z above a grounded infinite conducting plate, a negative induced charge will pool up beneath the point charge due to attraction. For the purposes of calculating the field above the plate, one can assume that there is a negative charge of equal magnitude z below the plate. In this situation, the net charge is zero because the conductor "canceled out" the point charge.

If a finite sphere is considered rather than an infinite plate, the induced charge q' becomes smaller and moves closer to the surface. For a sphere with radius R, the induced charge is given by

$$q' = -\frac{R}{R+d}q \tag{7}$$

where d is the distance between the dielectric charge and the surface of the conductor, and q is the dielectric charge, as is shown in Fig. 3. When d is much smaller than R, the induced charge is nearly equal and opposite to the dielectric charge and will cancel out its effect on the total charge. However, when d is comparable to R, the effect of the dielectric charge on the total charge is much more significant.

There are many differences between the electric field in the vicinity of a point charge and a conducting sphere, as well as the electric field in the vicinity of a charged solar panel and a conducting spacecraft bus, but there is still some intuition to gain from this simple analysis. The MOI predicts that, when the dielectric is very near the conductor, its charge will be mostly canceled out, regardless of how charged it is. Dielectric coatings sitting directly over conductors will likely not cause any significant changes for this reason. If the dielectric is far from a conductor, like a solar panel might be, then the effects are more significant. To understand how this simple principle applies to more complex spacecraft, numerical studies are performed next.

IV. Truth Model Development

The method of moments is used to create a truth model of the electric field in the vicinity of the spacecraft for a simpler MSM model to match. Prior work [19] has found that MSM models that match the E field also match the force and torque very well, and matching E fields solves a number of other optimization issues as well.

This is done for four spacecraft under three separate charging conditions. The first spacecraft (Fig. 4a) is a 3 m by 1 m box with a dielectric hovering 25.4 μm (~1 mil) above the top of the spacecraft. This serves as a model of the case where the MLI is stretched over the conducting exterior of the spacecraft. The small displacement off the surface is chosen to be a common thickness for MLI. The second spacecraft (Fig. 4b) is almost identical to the first, but the top conductor is removed and the dielectric is shifted down to be flush so that it is stretched over the perimeter of the conductor like the surface of a drum. The third spacecraft (Fig. 4c) has three panels made of dielectric so that it has equal area of the conductor and dielectric. The fourth and final spacecraft (Fig. 4d) is composed of five dielectric panels and a single conducting panel on the very bottom. All spacecraft are referred to with the shorthand "XcYd" where X is the number of conducting panels and Y is the number of dielectric panels, so the last spacecraft discussed can be indicated by 1c5d. These four spacecraft span the range from a small amount of dielectric completely on top of a conductor to almost all dielectric with very little conductor very far away.

In all subplots in Fig. 4, the conductor is charged to +30 kV and the dielectric to -250 nC/m^2. For some models (especially the 1c5d one), the peak charge per element goes up to 94 nC, but the color scale only extends up to 30 nC per element to better show the charge distribution. The positive charge concentrates near the negative dielectric in all cases. Consider the first two cases (Figs. 4a and 4b), which only differ by the inclusion of a conductor backing behind the dielectric. In the case without the backing, much more charge must accumulate on the side panels to cancel out the negative charge; whereas in the case with the backing, all the charge accumulates on that backing and is not seen. The other two cases (Figs. 4c and 4d) have even more positive charge accumulate to cancel out the large negative panels.

In addition to solving for the charge distribution, the electric field in the vicinity of the spacecraft is also found. The E field is computed at 30 points uniformly spread across each of 12 different spherical shells, ranging in radius from 3 to 25 m. The E field is computed for three different cases as well: the first, in which only the conductor is charged to +30 kV and the dielectric has no net charge (but has a high voltage due to its proximity to the dielectric); one in which the conductor is charged and the dielectric is additionally charged to -250 nC/m^2; and the last, in which the conductor is grounded (0 V) and the dielectric is charged. These 30 points per shell across 12 different shells for three different charging scenarios for four different spacecraft represent 4320 individual E field computations.

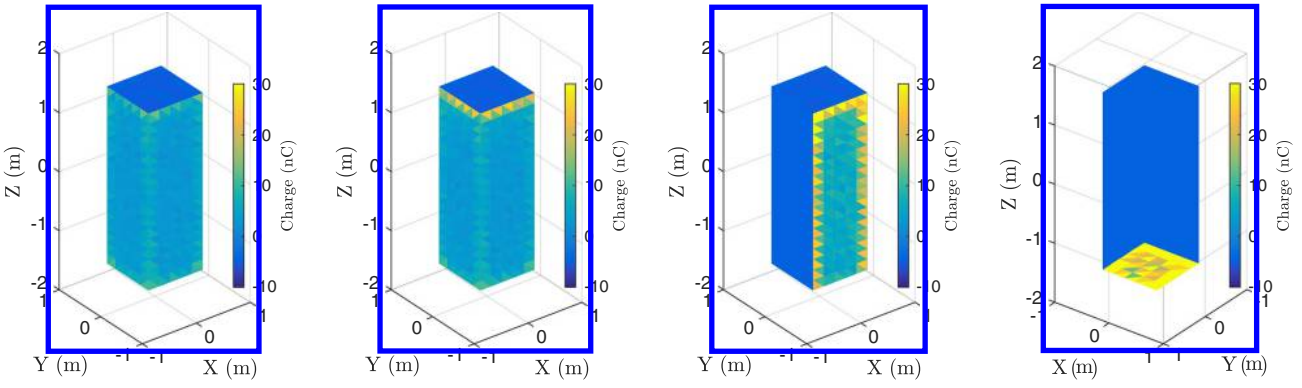

a) 6 conductors 1 dielectric **b) 5 conductors 1 dielectric** **c) 3 conductors and 3 dielectrics** **d) 1 conductor and 5 dielectrics**

Fig. 4 Four template spacecraft truth models computed using the method of moments.

V. Conductor Solutions

As a first attempt at modeling these spacecraft, the dielectric surfaces are ignored entirely and the optimization is done using a dataset where the dielectric is uncharged. This method has promise for the spacecraft with dielectrics close to conductors such as the 6c1d because of the image charges. A three-sphere MSM model, where all spheres are constrained to stay on the z axis but can change their height and radius, is optimized using only the conducting data for all spacecraft. The cost function is the average percent error of the E field the MSM model produces relative to the truth model. The optimizer changes the size and location of the three spheres to match the E field provided by the truth model as best it can. The final solution for the 3c3d spacecraft is shown in Fig. 5 with its three spheres constrained along the z axis. Because all three spheres have a tunable radius and height, there are six free parameters in this model.

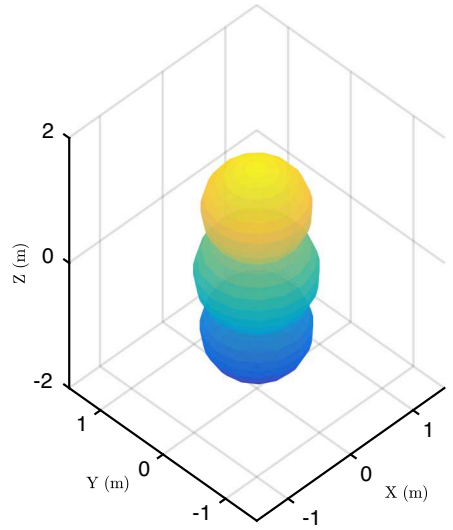

Fig. 5 Optimal MSM model for 3c3d spacecraft ignoring dielectrics.

This process of ignoring the dielectrics is applied to all four spacecraft, and their performances in both the conducting and mixed charging regimes are shown in Fig. 6. The performances are shown through the percent error between the E field predicted by the MSM model and the truth E field from the MOM truth file at each point: $E = 100\|\boldsymbol{E}_{\text{MSM}} - \boldsymbol{E}_{\text{MOM}}\|/\|E_{\text{MOM}}\|$. All MSM models have only conducting spheres and are optimized using just the conducting dataset (+30 kV and no dielectric charge).

The performance of the 6c1d model is shown using a violin plot in Fig. 6a. Violin plots are a good way to show a lot of data at once; they essentially show multiple histograms rotated by 90 deg. The width of each bar corresponds to the number of cases in the bin shown on the y axis for the case shown on the x axis. In the following violin plots, the cases correspond to how far away the E field is measured; the bins correspond to the percentage error (with reference to the MOM truth model); and the color corresponds to the charging scenario, with the dark blue being the conductor C and the aqua being the mixed case M. For the 6c1d spacecraft (Fig. 6a), the errors for the C and M cases are incredibly similar, and both are very good: they are almost always below 1% error and, after 10 m, they are always better than 0.1% error. They are similar because the induced charge on the top plate of the conductor almost entirely cancels out the dielectric charge, making it as though the charged dielectric is not even there.

Moving to the 5c1d case (Fig. 6b), the conducting regime errors are almost unchanged, but the mixed charging regime errors are larger. This is because the two cases are no longer as similar due to the lack of a top conducting panel to cancel out the dielectric charge. Despite this, the conductor only model has only a few percent error in the M category, which is more than accurate enough for many missions because voltage is often estimated only within a few hundred volts [24]. The 3c3d spacecraft (Fig. 6c) is slightly harder to model with mixed regime errors in the 10% range even though conductor errors are still very small. This is because much of the dielectric is much farther away from the conductor. Moving finally to the 1c5d case (Fig. 6d), the C errors are still very good, but the M errors have increased up to a 200% error.

From this analysis, it seems that one would not bother to model dielectrics for the 6c1d or the 5c1d, but one would probably do so for the 3c3d and definitely for the 1c5d. To expand this analysis to more continuous charging conditions, the dielectric charge density is swept

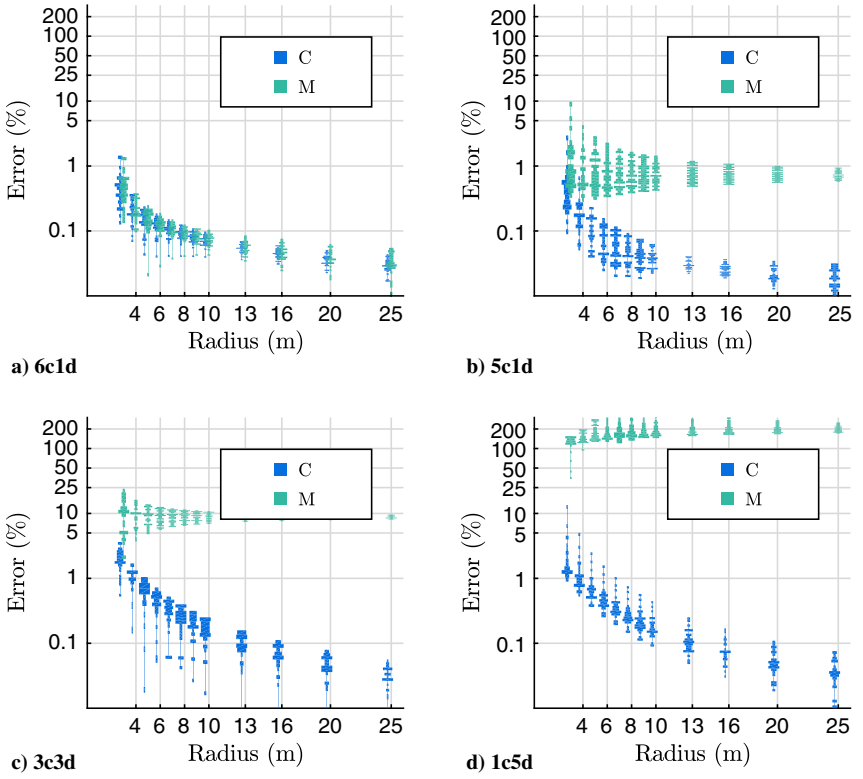

Fig. 6 Performance of a conductor-only MSM model in pure conducting C and mixed M charging regimes.

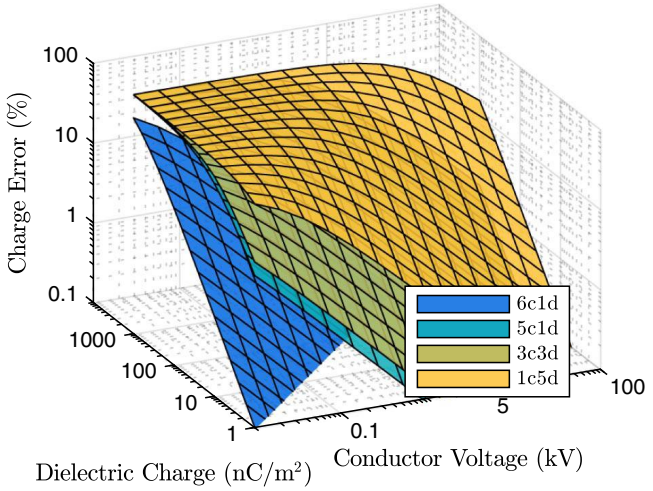

Fig. 7 Charge error as a function of voltage and dielectric charge density for four spacecraft.

from 1–1000 nC/m and the voltage is changed from 10 V to 100 kV for each spacecraft. For each charging condition, the charge percentage error is computed as $100(Q_C - Q_T)/(Q_T)$, where Q_C is the total charge found if the dielectric is ignored and Q_T is the true total charge. This charge error correlates with the percentage error when computing force in the far field, and it should be small to ensure accuracy. The charge error is always 100% when the voltage is zero because the conductor-only solution will always predict $Q_C = 0$, even if the total charge Q_T is negligible. Thus, this method for judging the charge error can produce misleading results when the voltage is small. The charge errors are shown in Fig. 7, where the different colors indicate different spacecraft.

In general, the charge errors grow as the dielectric charge is increased, which makes sense as the ignored charge becomes larger. The charge errors are also large when the voltage is low because they are percentage based. The 1c5d spacecraft has the worst errors, as expected, because it is mostly dielectric and has many panels that do not come close to the conductor. For this template spacecraft, errors will be large for almost all dielectric and conductor charge configurations. For the two intermediate spacecraft (the 3c3d and 5c1d), the performance is very similar. They both have charge errors larger than 10% if the dielectric charge is larger than 500 nC/m^2 when the voltage is 5 kV. The 6c1d spacecraft is the bounding case: neglecting dielectrics only introduces significant percentage errors when the spacecraft is at very low voltages, at which the actual charge and resulting force and torque will be very small and such errors are permissible.

This manner of analysis can be used to quickly check if dielectrics ought to be considered in an analysis. First the self- and mutual dielectric capacitances are found for the spacecraft in question. Next, the voltage and dielectric charge ranges are found; finally, the charge error is computed for the voltage and dielectric charge ranges. If the charge error is higher than the acceptable error for that mission, dielectrics must be included. This answers the first question: When ought dielectrics to be considered? Now, how to best model dielectrics is considered.

VI. Dielectric MSM Methodology

Dielectrics charge on much slower timescales than conductors because of their large mutual capacitance. Because of this, they are treated as known point charges rather than known voltages. To modify the conducting MSM to include dielectrics, the model is broken into two parts for the conductor and dielectric:

$$\begin{bmatrix} \boldsymbol{V}_C \\ \boldsymbol{V}_D \end{bmatrix} = \begin{bmatrix} S_C & S_M \\ S_M^T & S_D \end{bmatrix} \begin{bmatrix} \boldsymbol{Q}_C \\ \boldsymbol{Q}_D \end{bmatrix} \tag{8}$$

where the C and D subscripts denote the conductor and dielectric, respectively; and the M is for mutual. Because the voltage of the conductor and the charge of the dielectric are assumed known and the charge distribution for the conductor is sought, the top line of this equation is rearranged to give

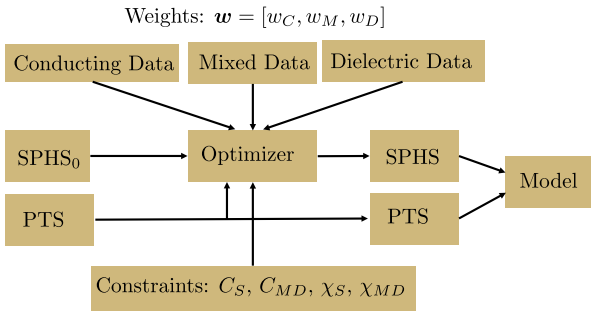

Fig. 8 Optimization scheme for dielectric MSM.

$$\boldsymbol{Q}_C = [S_C]^{-1}(\boldsymbol{V}_C - [S_M]\boldsymbol{Q}_D) \tag{9}$$

Then, the total charge $\boldsymbol{Q}$ can be formed as $\boldsymbol{Q} = [\boldsymbol{Q}_C, \boldsymbol{Q}_D]^T$. The force, torque, or E field is then computed as discussed in Sec. II.

When modeling conducting bodies, the MSM optimization problem is fairly simple: change the position and size of the spheres to best match the force, torque, or E field from a truth model. With dielectrics, there are a few changes: now, there are both conducting spheres and point charges which may be moved, and there are many different charging scenarios to consider when producing the truth model. With conductors, it does not matter what voltage is chosen for the truth model, as long as it is not zero. With dielectrics included, models that work well for a high-voltage case can perform very poorly for a high charge case.

To address the problem of optimizing for just one charging regime, three charging scenarios are included in the truth file; one with just the conductor charged and no charge on the dielectric, one with both the conductor and dielectric charged, and one with just the dielectric charged. Because using many point charges does not greatly slow down computation time (and to make the optimization easier), the point charges are uniformly distributed over the dielectric panels. This scheme is shown in Fig. 8.

An initial guess for the spheres location and radius (SPHS$_0$) is supplied to the optimizer. The optimizer uses the points model (PTS) along with the spheres model to compute the E field at all 30 points in all of the 12 shells for all three charging scenarios. The cost is computed from the average percentage error for all three charging scenarios and the weights. A selection of constraints, to be discussed later, can also be used to ensure behavior in the far field. The final spheres model is combined with the prescribed points model to make the full model for that spacecraft.

VII. Optimization Constraints

Prior work in optimizing MSM models for conductors [18,19] has shown that enforcing that the MSM model has the same self-capacitance as the object being modeled can make the optimization more robust and provides a guarantee of correctly modeling the force in the far field. The self-capacitance is a scalar parameter that determines how much charge is present at a given voltage. For a spacecraft with both dielectric and conducting components, the total charge is a function of both the conductor voltage and the dielectric charge. The total charge is the sum of the dielectric charge and the conductor charge:

$$Q = 1_{n_C}^T \boldsymbol{Q}_C + 1_{n_D}^T \boldsymbol{Q}_D \tag{10}$$

where the notation 1_n indicates a column vector of ones with n elements, and n_C and n_D denote the number of conducting and dielectric elements. Now, substitute in Eq. (9) for $\boldsymbol{Q}_C$ and rearrange

$$Q = 1_{n_C}^T [S_C]^{-1}(\boldsymbol{V}_C - [S_M]\boldsymbol{Q}_D) + 1_{n_D}^T \boldsymbol{Q}_D \quad = C_S V_C + C_{\mathrm{MD}} Q_D \tag{11}$$

where the self-capacitance C_S and mutual dielectric capacitance C_{MD} are defined as

$$C_S \equiv 1_{n_C}^T [S_C]^{-1} 1_{n_C} \tag{12}$$

$$C_{\mathrm{MD}} \equiv (1 - 1_{n_C}^T [S_C]^{-1} [S_M] 1_{n_D}^T / n_D) \tag{13}$$

The self-capacitance determines how sensitive the total charge is to the voltage on the conductor, and the mutual dielectric capacitance determines how sensitive the total charge is to the dielectric charge. If $C_{\mathrm{MD}} = 1$, then adding charge to the dielectric adds exactly that much to the total charge. If $C_{\mathrm{MD}} = 0$, then adding charge to the dielectric adds no charge at all to the total charge because the induced charge cancels it out. Referencing back to the MOI solution, $C_{\mathrm{MD}} \approx 1 - R/(R + d)$. So, when the dielectric is close to the conductor ($d \ll R$), C_{MD} will be close to zero, and the dielectrics will have minimal effects. When the dielectric is far from the conductor ($d \sim R$), C_{MD} will be close to one and dielectrics will play a larger role. Unlike the self-capacitance that has units of farads, C_{MD} is dimensionless and is always between zero and on.

The total charge is a zeroth-order moment of the charge distribution. The first-order moment of the charge distribution is the dipole $\boldsymbol{q}$. The dipole is a 3×1 vector formed by multiplying the total charge by a vector pointing from the center of the coordinate system (usually at the center of mass) to the center of the charge, and it was discussed in greater detail in Ref. [25]. MSM models that match the total charge and the dipole will correctly predict the torque as well as the force in the far field.

For a MSM model with both dielectric and conducting parts, the dipole is a combination of the dipole from both the dielectric and conducting portions:

$$\boldsymbol{q} = \boldsymbol{\chi}_S V + \boldsymbol{\chi}_{\mathrm{MD}} Q_D \tag{14}$$

where the parameters $\boldsymbol{\chi}_S$ and $\boldsymbol{\chi}_{\mathrm{MD}}$ are the self- and mutual susceptibilities defined by

$$\boldsymbol{\chi}_S \equiv [R_C][S_C]^{-1} 1_{n_C} \tag{15}$$

$$\boldsymbol{\chi}_{\mathrm{MD}} \equiv \frac{[R_D] 1_{n_D}}{n_D} - \frac{[R_C][S_C]^{-1}[S_M] 1_{n_D}}{n_D} \tag{16}$$

where $[R_C]$ and $[R_D]$ are matrices containing the location of every sphere/point in an MSM model or the centroid of every triangle in a MOM model for both the conductor and dielectric:

$$[R] = \begin{bmatrix} x_1 & \dots & x_N \\ y_1 & \dots & y_N \\ z_1 & \dots & z_N \end{bmatrix} \tag{17}$$

The self-susceptibility determines how sensitive the total dipole is to the conductor voltage, and the mutual susceptibility determines how sensitive it is to the dielectric charge. If the mutual susceptibility is small, the charge on the dielectric will not influence the dipole strongly. Once again, the units differ because the two susceptibilities multiply different quantities.

These four parameters (C_S, C_{MD}, $\boldsymbol{\chi}_S$, and $\boldsymbol{\chi}_{\mathrm{MD}}$) are all intrinsic and unchanging properties of a given spacecraft geometry. These constraints are enforced during optimization to understand how they affect the performance. Because these four constraints can be enforced in groups, there are 16 different unique sets of constraints that can be used. For each constraint set, the MSM solution is optimized for the 3c3d spacecraft using a prescribed points model for the dielectric that uses 36 points and a seven-sphere MSM model that has three spheres on each of the conductor panels and one along the central axis.

The results are shown in Fig. 9. The MSM solution for one of the 16 cases is shown in Fig. 9a. This particular optimization was constrained to match the self-capacitance and self-susceptibility, but not either of the mutual terms. The performance of this model is shown as a triple violin plot in Fig. 9b. The errors for all three scenarios decrease with distance, dropping below 1% at around 10 m for the dielectric case and near 7 m for the conductor and mixed case. The maximum error is near 10%, but that is only for the dielectric-only case at the closest distance. Because it would be tedious to show a triple violin plot for each of the 16 different constraint cases, the performance is reduced to two scalar values, this first of which is the mean of the errors for each field point at each radius and 11 each charging condition. This value is shown for all of the 16 constraint cases in Fig. 9c. The second one is introduced at the start of the next paragraph.

The first thing to notice is that the errors are all very good, regardless of the constraints used. The maximum mean error is 1.35%, which is less than all the other uncertainties in the system are likely to be. The lowest error is found with no constraints at all, which is expected because the optimizer has access to more solutions than the constrained solutions. In general, the leftmost and third-from-left columns are similar to each other and darker than the rest, indicating that the optimizer picks MSM models that match self-capacitance even if that constraint is not enforced. The first and third rows also have lower errors than the other rows, especially when combined with the first and third columns. This indicates that C_S and $\boldsymbol{\chi}_S$ are the most important parameters to match. Looking at the outside edge near the upper-left corner shows the effects of including just one constraint at a time. No constraints at all gives a mean error of 1.11%; just $\boldsymbol{\chi}_S$ gives 1.14%; $\boldsymbol{\chi}_{\mathrm{MD}}$ gives 1.16%; C_{MD} gives 1.17%; and C_S gives the same 1.11%. This analysis of looking at the constraints one at a time supports the idea that C_S and $\boldsymbol{\chi}_S$ are the most important parameters to match in order to predict the E fields well, which is a proxy for predicting forces and torques well.

The second scalar value to draw from the violin plots is the mean error for all charging conditions at 25 m. This final error should be more sensitive to enforcing constraints due to its distance and is shown in Fig. 9d. The first and third columns are even more dramatically better than the rest than in the mean error, as is the third row. Here, the lowest error comes from enforcing the self-susceptibility constraint: either with or without the self-capacitance. The mean and final error analyses both show that C_S and $\boldsymbol{\chi}_S$ are the most important constraints to enforce for this spacecraft. Enforcing both only hurts the mean error by 0.04%, and it provides a guarantee of performance in the far field.

This particular seven-sphere 36-point model has eight free parameters, which makes it possible to enforce any combination of constraints and still have many free parameters to tune for optimality. Despite this, it is still a very difficult optimization requiring very precise initial conditions. For more simple MSM models with fewer free parameters, it is not possible to enforce all of these constraints, depending on the number of free parameters. It is also possible that the constraints are not compliant for some MSM models; for example, a MSM model that had all spheres constrained on the z axis would never be able to match any nonzero x and y components of $\boldsymbol{\chi}_S$. For this model, constraints aid the solution because they are compliant. For other models, they are detrimental or impossible to enforce.

VIII. Performance and Time Analysis

The earlier section investigated the effect of constraints while keeping the model (3c3d spacecraft with seven spheres and 36 points) constant. This section uses no constraints, but it investigates the E field fitting performance while changing the spacecraft and its sphere and points model. For all spacecraft, the points are distributed equidistantly across the dielectric panels as shown in Fig. 9a. This

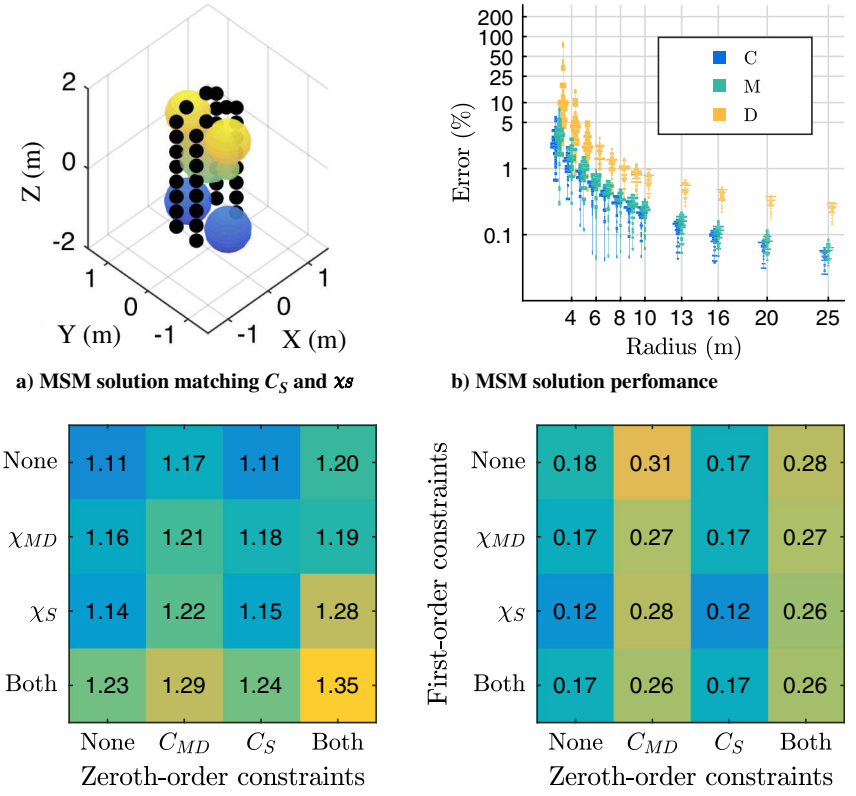

a) MSM solution matching C_S and χ_S **b) MSM solution perfomance**

c) Mean error **d) Final error**

Fig. 9 Effects of enforcing constraints.

model has two rows, which results in 36 points: one row gives 11 points, whereas 3 rows will give 75 points. For dielectric-heavy spacecraft (such as the 1c5d), there are naturally many more points than for conductor-heavy spacecraft (such as the 6c1d).

For all spacecraft, the spheres model uses a few spheres placed either along the z axis or in the plane of the conducting panels. The simplest model uses two spheres where both spheres have variable radii and position along the z axis. The next most complicated model has three spheres with variable radii and height for six total parameters. More advanced models have one sphere free to move along the z axis and a few rings of spheres centered on the panels that can change height and radius. Figure 9a shows a model for the 3c3d spacecraft with three rings of spheres along the vertical panels and one central sphere along the z axis, for a total of seven spheres. For the 1c5d spacecraft, none of the above models work well; so, one-, four-, and five-sphere models are made that keep all spheres in the $z = -1.5$ m plane. In total, 10 separate sphere models and 9 separate point models are considered for a total of 53 optimizations, which are shown in Fig. 10. If no points are used, the dielectric dataset is ignored because it will always give 100% error.

The first plot (Fig. 10a) shows how well different designs model the E field surrounding the 6c1d spacecraft. an earlier analysis found that dielectrics did not need to be modeled, and this analysis confirms that and finds that adding points actually hurts the solution. If no points are used, the mean errors are all less than 0.2%; but, if points are added, they jump up to at least 20%, and sometimes almost 100%. Among the conductor-only solutions, there is very little variation, with more spheres helping in general, except for the five-sphere model.

Moving to the 5c1d spacecraft (Fig. 10b), adding points still makes the solution worse but not by as much as the 6c1d. Ignoring the dielectric gets errors near 0.5%, but including them gets errors near 5%. In general, more spheres helps, with the exception of the five-sphere model, which appears to be an all-around bad model, regardless of the number of points used on both the 6c1d and 5c1d spacecraft. For both of these spacecraft, one ought to ignore the dielectrics entirely.

The 3c3d spacecraft (Fig. 10c) has equal area of the conductor and dielectric and has slightly smoother behavior. Ignoring dielectrics results in mean errors near 4%, and including them can either help or hurt this solution. For instance, including points makes the solution nearly three times worse for a two-sphere model but nearly three times better for a seven-sphere model. For any models with more than three spheres, dielectrics ought to be included. Except for the first row, more spheres and points both help the solution. Because the columns are more distinct than the rows, one can conclude that the number of spheres is more important than the number of points, although the jump from 0 to 11 and 11 to 36 points is significant.

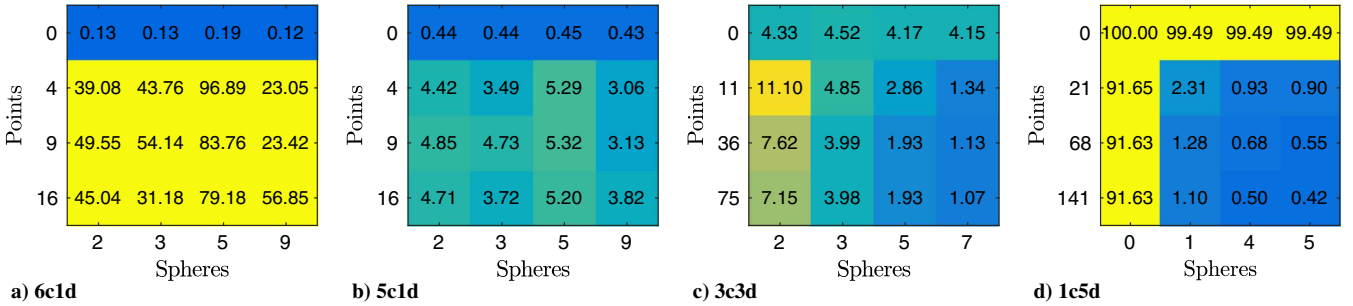

a) 6c1d **b) 5c1d** **c) 3c3d** **d) 1c5d**

Fig. 10 Mean error of E field fitting for different sphere and point models.

Finally, the 1c5d spacecraft mean error is shown in Fig. 10d. Because this spacecraft is virtually all dielectric, a points-only solution is also considered. Both the points and only-spheres cases perform poorly with errors near 100%. For the cases with both spheres and points, the errors are much better; and they decrease as spheres and points are added. In contrast to the 3c3d spacecraft, the rows are just as distinct as the columns, which indicate that adding points for this spacecraft is more valuable than on the 3c3d, which makes sense because the dielectric is larger and plays a larger part in the E field.

Overall, the two spacecraft for which dielectrics ought not be included are the easiest to model with errors always less than 0.5%. The 3c3d spacecraft provides an intermediate case where the number of spheres being used determines whether points ought to be used. For all spacecraft, a model exists that keeps the average error below 1.5%, which is likely lower than other errors expected in the system.

Many of the proposed applications of electrostatic force modeling must evaluate quickly as well as accurately. To investigate the trade space between accuracy and time, the number of arithmetic operations needed is found. For an MSM model with n conducting spheres and m dielectric point charges, the number of operations N required to find the charge at each node [using Eq. (9)] is

$$N = \frac{2}{3}n^3 + \frac{11}{2}n^2 - \frac{25}{6}n + 2 \text{ mn} \tag{18}$$

if using Gauss–Jordan elimination for the matrix inverse.

This measure is not the full number of computations that must occur to compute the electrostatic force or torque, but it is the most time-intensive step. All other steps will involve the number of points and spheres in both models, and are therefore more difficult to include without introducing unnecessary complexity.

The mean error function is plotted in Fig. 11 for all spacecraft and all models as a function of operations, which are a proxy of computer time. The small numbers indicate which model is used: a pair of i, j indicates a model with i spheres and j points, and the color indicates the spacecraft. For the 6c1d and 5c1d spacecraft, only the conductor-only solution is shown because the others have poor performance. For the other two spacecraft, all the designs are shown with lines indicating models with the same number of spheres. Additionally, a boundary line and shading is used to indicate the likely Pareto frontier, which here is the boundary line that allows a designer to choose the best tradeoff between accuracy and speed.

It is now clear that the 3c3d spacecraft is the least accurate, but it still has a mean error below 10% for all but one design. The 1c5d spacecraft follows a much tighter boundary and is more accurate while requiring roughly the same computational effort. Lastly, the two conductor-only spacecraft are not strong functions of the computational effort but are very accurate, no matter which model is used. This plot, or others like it, could be used to decide which model to use for a particular mission with known accuracy and speed constraints.

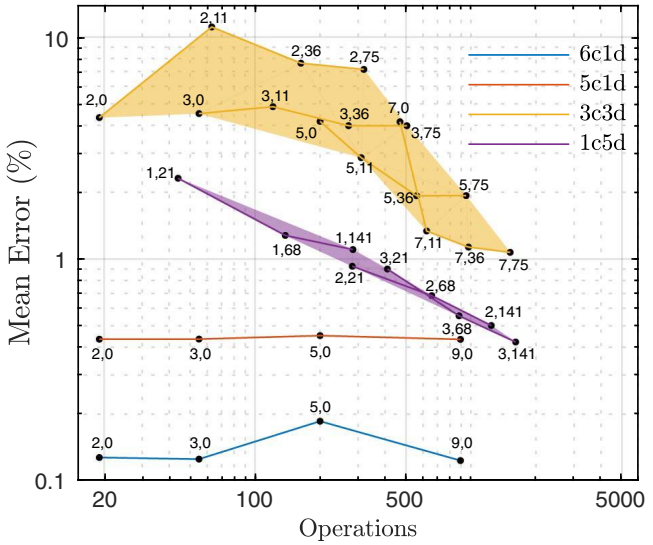

Fig. 11 Mean error for all spacecraft as a function of arithmetic operations.

IX. Conclusions

This paper seeks to answer two questions: First, "When ought dielectrics be modeled?" and second, "How can dielectrics be modeled in multisphere method (MSM)?" The first question is answered through an analysis of the mutual dielectric capacitance, as well as by including and neglecting dielectrics for certain models. For the four spacecraft analyzed, two of them do not need to have their dielectric components modeled. In fact, including them makes the solution worse. For the other two, ignoring dielectrics can lead to errors in the E field of hundreds of percent. The mutual dielectric capacitance analysis provides the analytical tools to extend this to other spacecraft than the four analyzed.

The second question is answered by using a point charge model for the dielectric portions of the spacecraft. When optimizing the full model, the points are included but not allowed to be varied; and three datasets that include conductor-only, mixed, and dielectric-only cases are included. Constraints can help enforce the far-field behavior without hurting the overall performance for some models, but the constraints are not always compliant for all models and all spacecraft. When optimized without any constraints, the predicted E field only differs from the truth model by less than 10%: often less than 1%. The conductor solutions are the most accurate, with the 1c5d and 3c3d following behind. Overall, modeling dielectrics using MSM is feasible, and the errors for the cases considered here are less than other errors expected in the system.

Acknowledgments

This work is supported by U.S. Air Force Office of Scientific research grant number FA9550-15-1-0407. Thank you to Miles Bengtson, Kieran Wilson, and Jordan Maxwell for fruitful research conversations.

References

[1] Olsen, R. C., "The Record Charging Events of ATS-6," *Journal of Spacecraft and Rockets*, Vol. 24, No. 4, 1987, pp. 362–366. doi:10.2514/3.25925

[2] Früh, C., Ferguson, D., Lin, C., and Jah, M., "The Effect of Passive Electrostatic Charging on Near-Geosynchronous High Area-to-Mass Ratio Objects," *Proceedings of AAS Space Flight Mechanics Meeting*, Santa Fe, NM, 2014, pp. 3121–3137.

[3] Hughes, J., and Schaub, H., "Rapid Charged Geosynchronous Debris Perturbation Modeling of Electromagnetic Disturbances," *Journal of Astronautical Sciences*, Vol. 65, No. 2, June 2018, pp. 135–156.

[4] Paul, S. N., and Früh, C., "Space-Object Charging and Its Effect on Orbit Evolution," *Journal of Guidance, Control, and Dynamics*, Vol. 40, No. 12, Dec. 2017, pp. 3180–3198.

[5] Hughes, J., and Schaub, H., "Space Weather Influence on Electromagnetic Geosynchronous Debris Perturbations Using Statistical Fluxes," *AGU Space Weather*, Vol. 16, No. 4, 2018, pp. 391–405. doi:10.1002/swe.v16.4

[6] Berryman, J., and Schaub, H., "Analytical Charge Analysis for Two- and Three-Craft Coulomb Formations," *Journal of Guidance, Control, and Dynamics*, Vol. 30, No. 6, 2007, pp. 1701–1710. doi:10.2514/1.23785

[7] Hogan, E., and Schaub, H., "Collinear Invariant Shapes for Three-Craft Coulomb Formations," *Acta Astronautica*, Vol. 72, March–April 2012, pp. 78–89. doi:10.1016/j.actaastro.2011.10.020

[8] Inampudi, R., and Schaub, H., "Optimal Reconfigurations of Two-Craft Coulomb Formation in Circular Orbits," *Journal of Guidance, Control, and Dynamics*, Vol. 35, No. 6, 2012, pp. 1805–1815. doi:10.2514/1.56551

[9] Bengtson, M., Wilson, K., Hughes, J., and Schaub, H., "Survey of the Electrostatic Tractor Research for Reorbiting Passive GEO Space Objects," *Astrodynamics*, Vol. 2, No. 4, Dec. 2018, pp. 291–305. doi:10.1007/s42064-018-0030-0

[10] Schaub, H., and Moorer, D. F., "Geosynchronous Large Debris Reorbiter: Challenges and Prospects," *Journal of the Astronautical Sciences*, Vol. 59, Nos. 1–2, 2014, pp. 161–176.

[11] Bennett, T., and Schaub, H., "Touchless Electrostatic Three-Dimensional Detumbling of Large GEO Debris," *Journal of Astronautical Sciences*, Vol. 62, No. 3, 2015, pp. 233–253.

[12] Bennett, T., Stevenson, D., Hogan, E., McManus, L., and Schaub, H., "Prospects and Challenges of Touchless Debris Despinning Using Electrostatics," *Advances in Space Research*, Vol. 56, No. 3, 2015, pp. 557–568.
doi:10.1016/j.asr.2015.03.037

[13] Bennett, T., and Schaub, H., "Capitalizing on Relative Motion in Electrostatic Detumbling of Axi-Symmetric Geo Objects," *6th International Conference on Astrodynamics Tools and Techniques (ICATT)*, Darmstadt, Germany, 2016, https://indico.esa.int/event/111/overview.

[14] Hogan, E., and Schaub, H., "Relative Motion Control for Two-Spacecraft Electrostatic Orbit Corrections," *Journal of Guidance, Control, and Dynamics*, Vol. 36, No. 1, 2013, pp. 240–249.
doi:10.2514/1.56118

[15] Gibson, W. C., *The Method of Moments in Electromagnetics*, Chapman and Hall, Boca Raton, FL, 2007.

[16] Feng, J. Q., "Electrostatic Interaction Between Two Charged Dielectric Spheres in Contact," *Physical Review E*, Vol. 62, No. 2, 2000, pp. 2891–2897.
doi:10.1103/PhysRevE.62.2891

[17] Stevenson, D., and Schaub, H., "Multi-Sphere Method for Modeling Electrostatic Forces and Torques," *Advances in Space Research*, Vol. 51, No. 1, 2013, pp. 10–20.
doi:10.1016/j.asr.2012.08.014

[18] Chow, P., Hughes, J., Bennett, T., and Schaub, H., "Automated Sphere Geometry Optimization for the Volume Multi-Sphere Method," *AAS/AIAA Spaceflight Mechanics Meeting*, AAS Paper 16-472, 2016.

[19] Ingram, G., Hughes, J., Bennett, T., Reily, C., and Schaub, H., "Volume Multi-Sphere-Model Development Using Electric Field Matching," *Journal of Astronautical Sciences*, Vol. 65, No. 4, 2018, pp. 377–399.

[20] Hughes, J., and Schaub, H., "Effects of Charged Dielectrics on Electrostatic Force and Torque," *International Workshop on Spacecraft Formation Flying*, 2017.

[21] Jackson, J. D., *Classical Electrodynamics*, Wiley, New York, 1999.

[22] Lekner, J., "Electrostatics of Two Charged Conducting Spheres," *Proceedings of the Royal Society of London, Series A: Mathematical, Physical and Engineering Sciences*, Vol. 468, No. 2145, 2012, pp. 2829–2848.
doi:10.1098/rspa.2012.0133

[23] Metzger, P., and Lane, J., "Electric Potential due to a System of Conducting Spheres," *Open Applied Physics Journal*, Vol. 2, No. 1, 2009, pp. 32–48.
doi:10.2174/1874183500902010032

[24] Lai, S. T., *Fundamentals of Spacecraft Charging: Spacecraft Interactions with Space Plasmas*, Princeton Univ. Press, Princeton, NJ, 2011.

[25] Hughes, J., and Schaub, H., "Spacecraft Electrostatic Force And Torque Expansions Yielding Appropriate Fidelity Measures," *Journal of the Astronautical Sciences*, 2019, pp. 1–22.
doi:10.1007/s40295-019-00154-7

D. P. Thunnissen
Associate Editor